Coordinated control of a series-parallel hybrid electric bus during EV/HEV mode transition

LEI WANG, YONG ZHANG, JIE SHU, CHENG-LIANG YIN
National Engineering Laboratory for Automotive Electronic Control Technology
Shanghai Jiao Tong University
800 Dongchuan Road, Minhang District, Shanghai
CHINA
sanshes2003@yahoo.com.cn

Abstract: - Hybrid electric buses have been a promising technology to improve fuel economy and vehicle drivability. Due to the distinct transient response characteristics between different power sources and the discontinuity of the transmitted clutch torque, the output torque fluctuations of hybrid powertrains and the resulting vehicle jerks may occur during mode transitions, especially for the transition from the EV (electric vehicle) mode to the HEV (hybrid electric vehicle) mode. Aiming at achieving a smooth transition from the EV mode to the HEV mode for a series-parallel hybrid electric bus, this paper proposes a transient control strategy to coordinate the diesel engine and the motors during the transition process. The EV/HEV mode-transition control strategy is developed according to the operating status of the clutch, and the engine throttle is restricted during the transition process. In this control strategy, a fuzzy adaptive inference system is developed to estimate the difference between the actual and target engine torques. Then, the estimated torque difference is incorporated with a sliding mode controller to regulate the output torques of the integrated starter generator (ISG)and the traction motor (TM) to reduce the torque fluctuations in the powertrain. A simulation is performed using a forward-facing HEV model to validate the effectiveness of the proposed control strategy, and the results show significant reductions in torque fluctuations and vehicle jerks during the EV/HEV mode transition.

Key-words: - series-parallel hybrid electric bus; EV/HEV mode transition; transient response; fuzzy adaptive sliding mode control; coordinated control

1 Introduction

Increasingly stringent requirements on the fuel consumption and emissions for vehicles have spurred the development of vehicles with hybrid powertrains, especially for heavy-duty vehicles with high fuel consumption, such as city buses [1,2,3]. Hybrid electric vehicle (HEV) technology offers the potential for reducing fuel consumption and improving passenger comfort as it can coordinate the overall hybrid powertrain to improve fuel efficiency and vehicle drivability [1,2]. By bringing together an electrical propulsion system with a conventional internal combustion engine (ICE) propulsion system, a series-parallel HEV can select electric vehicle (EV) mode during low-speed driving and can select hybrid electric vehicle (HEV) mode during high-speed and accelerating driving to lower fuel consumption and emissions while satisfying the power demand. During the transition process from the EV mode to the HEV mode, the clutch should be engaged, and the engine should be started and coupled to the drivetrain. However, the transmitted torque of the clutch is discontinuous and changes sharply, and the transient response characteristics of the engine and the motor are distinct [4-8]. Thus, the output torque fluctuations of the hybrid powertrain and vehicle drivability deterioration may occur in the transient process of EV/HEV mode transition. Therefore, the coordinated control of the hybrid powertrain to reduce the output torque fluctuations and to achieve a smooth mode transition is an important subject concerning the series-parallel HEV control issues.

Thus far, only a few research studies have been proposed to address the problem of mode transitions of HEVs. The algorithms, which have been utilised for the coordinated control of hybrid powertrains during mode transitions, include the model predictive control approach, the on-board engine torque estimation approach, and the disturbance compensation approach [4-14]. The coordinated control strategy using the model predictive control approach [9-12] dealt with the problem of mode transition from electric launch to parallel hybrid operation for a parallel HEV. In this strategy, the dynamic behaviour of the HEV was described by a

simplified model, and the transition process from the EV mode to the HEV mode was divided into the engine start phase, the clutch engagement phase, and the parallel hybrid phase. The target torques of the engine and the motor during the engine start and the clutch engagement phases were determined using the optimal control theory. While during the parallel hybrid phase, the control actions were given by the core energy management strategy. The research result demonstrated that a seamless transition could be achieved. However, the main drawback of this approach is that it does not take into account the transient response characteristics of the engine and the motor. For a turbocharged diesel engine, the response time for the target torque is much longer than that of a motor. The coordinated control strategy using the on-board engine torque estimation approach [6-8] was based on the dynamic characteristics of both the engine and the motor. In this strategy, an engine torque observer was built based on the mean value engine model approach or the instantaneous crankshaft speed approach to give a prediction of the dynamic engine torque, and then, the motor torque was regulated to compensate for the disparity between the actual and target engine torques during mode transitions. The main problem with this approach is that the coordinated control performance during mode transitions completely depends on the predictive accuracy of the dynamic engine torque. The coordinated control strategy using the disturbance compensation approach [14] considered the disturbances in the engine and the clutch. The disturbances were estimated by using a disturbance observer, which is based on the state equations of the drivetrain. Then, the estimated disturbances were compensated for by the belt-driven starter generator (BSG) or the traction motor control. Thus, the estimation accuracy of the disturbances directly influenced the control accuracy of the mode transition. Moreover, in this strategy, the engine did not output power until the last phase of the mode transition, which is not conducive to the reduction of the vehicle response time.

This paper proposes a coordinated control strategy based on the fuzzy adaptive sliding mode control for a series-parallel hybrid electric bus to achieve a smooth transition from the EV mode to the HEV mode. In this study, the transient response characteristics of the engine and the motor as well as the friction-introduced discontinuity of the clutch torque are taken into account. The EV/HEV mode-transition control strategy is developed according to the operating status of the clutch, and the engine throttle is restricted during the transition process to suppress the engine's transient operation and fuel enrichment [7,8,13]. A fuzzy adaptive inference system is developed to estimate the difference between the actual and desired engine torques. Then, the estimated torque difference is incorporated with a sliding mode controller to regulate the output torques of the integrated starter generator (ISG) and the traction motor (TM) to reduce the torque fluctuations of the powertrain. A simulation is performed using a forward-facing HEV model, and the results presented validate the effectiveness of the proposed control strategy.

2 Hybrid system architecture

The architecture of the powertrain of the series-parallel hybrid electric bus considered here is shown in Fig.1, and the basic parameters of the vehicle are listed in Table 1.

Table 1. Main specifications of the vehicle

Item	*Value*
Curb/Gross weight (kg)	12200/17000
Wheel base (m)	5.8
Tire rolling radius (m)	0.508
Frontal area (m^2)	7.5
Aerodynamic drag coefficient	0.62

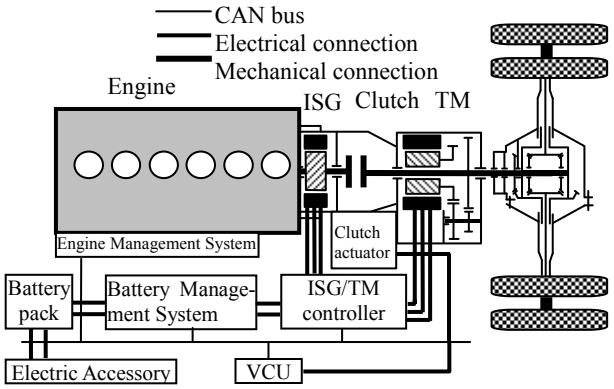

Fig. 1 Schematic of the hybrid system architecture

As is shown in Fig. 1, the powertrain of the HEV consists of a 6-cylinder turbocharged diesel engine, an ISG motor, a TM, a torque coupler, and an electronically controlled clutch. The engine is directly connected to the rotor of the ISG, then to the input shaft of the clutch. The TM is attached to the output shaft of the clutch and is coupled to the shaft via the torque coupler at a constant gear ratio. The clutch serves as a configuration switch component to form either an electric vehicle configuration or a hybrid electric vehicle configuration. In the EV mode, the clutch is disengaged, and the vehicle is driven by the TM alone with the electric energy from the battery, while in the HEV mode, the clutch is

engaged, and the vehicle is driven by the TM and the engine simultaneously. The vehicle control unit (VCU) is utilised to determine the most appropriate drive mode and the most fuel-efficient power split between the power sources. Meanwhile, the coordinated control for the EV/HEV mode transition is implemented by the VCU.

3 HEV simulation model

A forward-facing model of the hybrid bus is built in MATLAB/Simulink to simulate the behaviour of the vehicle and to validate the effectiveness of the coordinated control strategy proposed hereafter. This model includes the hybrid vehicle components, a driver, and the driving environment and is built on the basis of the energy flow given in Fig. 1. Details of the HEV model will be discussed in the following sections.

3.1 Turbocharged diesel engine model

The engine model in a forward-facing HEV simulation model recreates the characteristics of the engine, such as the fuel consumption and output torque. In this study, a mean value engine model is utilised for the transient operation of the selected turbocharged diesel engine. The time scale for a mean value engine model is on the order of 3 to 5 revolutions. Thus, such model is fast enough to give an accurate prediction of the overall dynamic engine operation [15]. The mean value engine model consists of a series of sub-systems. Such sub-systems include the compressor, the turbine, the intake manifold, the exhaust manifold, the intercooler, and the engine itself. The air flow and the temperature dynamics in the intake and exhaust manifolds are described by first-order differential equations based on the energy- and mass-conservation, and the pressure is deduced from the ideal gas law. Moreover, the volumetric and thermal efficiencies of the model are described by the characteristic maps based on the experimental results. Detailed descriptions of the mean value model for a four-stroke diesel engine are available in [15-17].

3.2 Electric machine model

Both the ISG and the TM utilised in the hybrid bus can operate in motor and generator modes. The simulation model of the electric machines in this study is used to calculate the actual output torque $M_{m,act}$ and the desired current at the motor link I_m based on the torque command $M_{req,m}$, the motor link voltage V_m, and the revolution speed of the rotor ω_m.

The behaviours of the electric machines are described by the characteristic maps based on the experimental data, which include the maximum and continuous torques as a function of speed, as well as a two-quadrant efficiency map as a function of speed and output torque. Like the engine, the required output torque $M_{req,m}$ of the motor are also determined by the VCU. A response time r_m is introduced to simulate the dynamic process for the motor to build up the full torque. Furthermore, the torque delivered by the motor should be limited by the maximum operating power P_{max}. Detailed calculation processes for P_{max} are available in [1,2,18]. Then, the actual operating torque $M_{m,act}$ that the motor can deliver is

$$M_{m,act} = \min\left(\frac{1}{r_m} e^{-\frac{t}{r_m}} \cdot M_{req,m}, \frac{P_{\max}}{9549\omega_m}\right) \quad (1)$$

The desired current at the motor link can be calculated as follows:

$$I_m = \begin{cases} \dfrac{M_{m,act}\omega_m}{9549 V_m \eta_m} & \text{(the motor mode)} \\ \dfrac{M_{m,act}\omega_m \eta_m}{9549 V_m} & \text{(the generator mode)} \end{cases} \quad (2)$$

where η_m is the electric motor operating efficiency interpolated from the efficiency map.

3.3 Clutch model

The clutch model here is used to calculate the transmitted torque under various operating statuses. The engagement and disengagement processes of the clutch consist of three statuses: the unlocked status, the slipping status, and the locked status [1,2,18,19]. The operating status of the clutch is determined by the normalised clutch release displacement D_n and the relative speed of the clutch ω_{rel}. For the unlocked status (when D_n=1), no torque is transmitted by the clutch. For the slipping status (when D_n<1 and ω_{rel}≠ 0), the transmitted torque of the clutch M_{cl} can be calculated as follows [1,2,19]:

$$M_{cl} = [\mu_{sl} + (\mu_{st} - \mu_{sl}) \cdot e^{-\frac{(|\omega_{rel}|G_{cl})}{\mu_{st}-\mu_{sl}}}] \cdot r_{cl} \cdot F_{cn} \cdot N_{cl} \cdot sign(\omega_{rel}) \quad (3)$$

For the locked status (when R_n<1 and ω_{rel}=0), the range of M_{cl} can be given by the following equation:

$$M_{cl} = [-\mu_{st} \cdot r_{cl} \cdot F_{cn} \cdot N_{cl} \quad \mu_{st} \cdot r_{cl} \cdot F_{cn} \cdot N_{cl}] \quad (4)$$

where μ_{sl} is the slip friction coefficient of the clutch; μ_{st} is the static friction coefficient of the clutch; G_{cl} is the friction gradient; r_{cl} is the effective friction

radius; N_{cl} is the number of the friction surface; F_{cn} is the normal force on the clutch plate and is exerted by the diaphragm spring.

The engagement and disengagement of the clutch are achieved by a pneumatic actuator in this study. A schematic of the pneumatic actuator of the clutch is shown in Fig. 2. The actuator is controlled by the VCU via the two on-off valves. Because the clutch should be engaged during the EV/HEV mode transition, only the engagement process of the clutch is analysed here. To engage the clutch, valve 1 should be turned off, while valve 2 should be turned on. The clutch release displacement D can be calculated as follows [20,21]:

$$\begin{cases} \dfrac{dp}{dt} = \dfrac{\gamma p}{(D_0 - D)}\dfrac{dD}{dt} - \dfrac{\gamma RTm'_{out}}{A(D_0 - D)}\left(\dfrac{p}{p_i}\right)^{\frac{\gamma-1}{\gamma}} \\ m_{cl}\dfrac{d^2D}{dt^2} + c_{cl}\dfrac{dD}{dt} = P_a A + F_c - PA \end{cases} \quad (5)$$

where p and p_i are the instantaneous pressure and the initial pressure of the cylinder, respectively. m_{cl} and c_{cl} are the equivalent mass and the damping coefficient of the clutch release bearing, respectively. γ is the adiabatic coefficient of the air; T is the temperature of the air; R is the ideal gas constant; A is the cross-sectional area of the piston; D_0 is the maximum deformation on the small end of the diaphragm spring; p_a is the atmospheric pressure; F_c is the force exerted by the diaphragm spring. m'_{out} is the mass flow rate of the air and can be calculated by the following equation [20,21]:

$$m'_{out} = \begin{cases} A_v p\sqrt{\dfrac{2\gamma}{RT(\gamma-1)}\left[\left(\dfrac{p_a}{p}\right)^{\frac{2}{\gamma}} - \left(\dfrac{p_a}{p}\right)^{\frac{\gamma+1}{\gamma}}\right]}, & \left[\dfrac{p_a}{p} > \left(\dfrac{2}{\gamma+1}\right)^{\frac{\gamma}{\gamma-1}}\right] \\ A_v p\sqrt{\dfrac{\gamma}{RT}\left(\dfrac{2}{\gamma+1}\right)^{\frac{\gamma+1}{\gamma-1}}}, & \left[\dfrac{p_a}{p} \le \left(\dfrac{2}{\gamma+1}\right)^{\frac{\gamma}{\gamma-1}}\right] \end{cases} \quad (6)$$

where A_v is the cross-sectional area of valve 2.

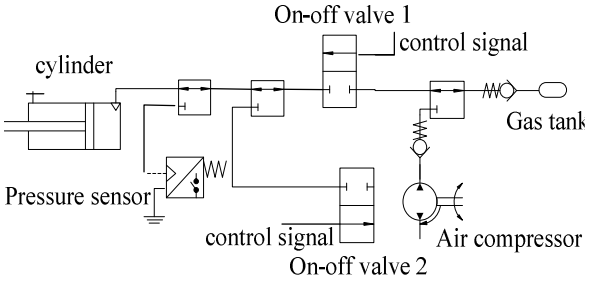

Fig. 2 Schematic of the pneumatic actuator

3.4 Longitudinal dynamic model

A simplified longitudinal dynamic model of the target hybrid bus is shown in Fig. 3. In this figure, J_{wh_veh} is the total inertia of the wheels and the effective vehicle inertia acting on the wheels; J_{TM} is the inertia of the TM; J_{en_isg} is the total inertia of the engine and the ISG; J_c and J_0 are the inertias of the TM reducer and the final drive, respectively; J_{cl_in} and J_{cl_out} are the inertias of the drive side and the driven side of the clutch, respectively; θ_1, θ_2, and θ_3 are the angular displacements of the input shaft of the clutch, the output shaft of the clutch, and the wheel, respectively; b_{TM} is the motor friction coefficient; b_{en_isg} is the total internal friction coefficient of the engine and the ISG; k_{da} and b_{da} are the equivalent stiffness and the damping coefficient of the drive axle; i_c and i_0 are the gear ratios of the TM reducer and the final drive, respectively.

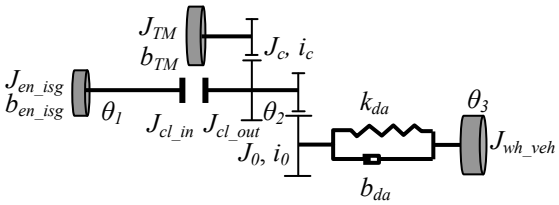

Fig. 3 Longitudinal dynamic model of the HEV

Considering the operating status of the clutch, the longitudinal dynamic equations for the hybrid bus can be expressed as follows.

1) For the unlocked status of the clutch,

$$\begin{cases} (J_{en\_isg} + J_{cl\_in})\ddot{\theta}_1 + b_{en\_isg}\dot{\theta}_1 = M_{en} + M_{isg} \\ (i_c^2 J_{TM} + J_c + J_{cl\_out} + \dfrac{1}{i_0^2}J_0)\ddot{\theta}_2 + i_c^2 b_{TM}\dot{\theta}_2 + \dfrac{1}{i_0}k_{da}\left(\dfrac{1}{i_0}\theta_2 - \theta_3\right) \\ + \dfrac{1}{i_0}b_{da}\left(\dfrac{1}{i_0}\dot{\theta}_2 - \dot{\theta}_3\right) = i_c M_{TM} \\ J_{wh\_veh}\ddot{\theta}_3 = k_{da}\left(\dfrac{1}{i_0}\theta_2 - \theta_3\right) + b_{da}\left(\dfrac{1}{i_0}\dot{\theta}_2 - \dot{\theta}_3\right) - M_L \end{cases} \quad (7)$$

2) For the slipping status of the clutch,

$$\begin{cases} (J_{en\_isg} + J_{cl\_in})\ddot{\theta}_1 + b_{en\_isg}\dot{\theta}_1 = M_{en} + M_{isg} - M_{cl} \\ (i_c^2 J_{TM} + J_c + J_{cl\_out} + \dfrac{1}{i_0^2}J_0)\ddot{\theta}_2 + i_c^2 b_{TM}\dot{\theta}_2 + \dfrac{1}{i_0}k_{da}\left(\dfrac{1}{i_0}\theta_2 - \theta_3\right) \\ + \dfrac{1}{i_0}b_{da}\left(\dfrac{1}{i_0}\dot{\theta}_2 - \dot{\theta}_3\right) = i_c M_{TM} + M_{cl} \\ J_{wh\_veh}\ddot{\theta}_3 = k_{da}\left(\dfrac{1}{i_0}\theta_2 - \theta_3\right) + b_{da}\left(\dfrac{1}{i_0}\dot{\theta}_2 - \dot{\theta}_3\right) - M_L \end{cases} \quad (8)$$

3) For the locked status of the clutch,

$$\begin{cases} (i_c^2 J_{TM} + J_c + J_{cl\_out} + \dfrac{1}{i_0^2}J_0 + J_{en\_isg} + J_{cl\_in})\ddot{\theta}_2 + (i_c^2 b_{TM} + b_{en\_isg})\dot{\theta}_2 \\ + \dfrac{1}{i_0}k_{da}\left(\dfrac{1}{i_0}\theta_2 - \theta_3\right) + \dfrac{1}{i_0}b_{da}\left(\dfrac{1}{i_0}\dot{\theta}_2 - \dot{\theta}_3\right) = i_c M_{TM} + M_{en} + M_{isg} \\ J_{wh\_veh}\ddot{\theta}_3 = k_{da}\left(\dfrac{1}{i_0}\theta_2 - \theta_3\right) + b_{da}\left(\dfrac{1}{i_0}\dot{\theta}_2 - \dot{\theta}_3\right) - M_L \end{cases} \quad (9)$$

where M_{en}, M_{isg}, M_{TM}, and M_{cl} are the engine torque, the ISG torque, the TM torque, and the clutch torque, respectively; M_L is the load torque. Due to the strong

nonlinear attributions of the tires, it is very difficult to build a perfect model to predict the dynamic performance of the tires. Some studies on the control of longitudinal dynamics [22-24] have been implemented while ignoring the wheel slip, and the effectiveness of those methods has been validated by experiments. Therefore, the vehicle velocity v can be defined as:

$$v = \dot{\theta}_3 \cdot r_r \tag{10}$$

where r_r is the tire rolling radius.

Additionally, models for the driver and battery are included in the HEV simulation model. A PID controller is used to simulate the driver, and an equivalent circuit model for the battery is adopted [25,26]. The Chinese Transit Bus Drive Cycle (CTBDC) is used to represent the most frequent drive conditions of the bus.

4 Coordinated control strategy development

To reduce fuel consumption and emissions, the hybrid bus is driven in the EV mode for low-speed driving conditions, and the hybrid bus is driven in the HEV mode for high-speed or accelerating driving conditions. The threshold velocity for the EV/HEV mode transition and the target torques of the engine, the ISG, and the TM during the mode transition are determined by the energy management strategy (EMS) in the VCU. In this study, a real-time suboptimal EMS is used [27], and the coordinated control strategy for the EV/HEV mode transition is developed on the basis of the predefined EMS.

Because the energy management strategy disregards the transient response characteristics of the power sources and the discontinuity of the clutch torque [33-35], the output torque fluctuations and the resulting vehicle jerks would occur if the vehicle control actions are directly given by the EMS during the EV/HEV mode transition. Consequently, a coordinated control is required to achieve a smooth transition. In this study, the response time for the target torque of the turbocharged diesel engine is on the order of 1 to 3 seconds, while the torque response times of the ISG and the TM are several milliseconds. Thus, the difference between the actual and target engine torques is regarded as a disturbance to the drivetrain, and the output torques of the ISG and the TM are regulated to reduce the torque fluctuations of the powertrain.

Due to the robustness against external disturbances and parameter variations, sliding mode control has been gaining popularity in automotive applications. However, the major drawback of this method is the chattering problem. One approach to reducing the chattering involves introducing a boundary layer around the switching surface and using a continuous control within the boundary layer [28,29,32]. In this study, a fixed-boundary-layer sliding mode controller (SMC) using a sat function is designed for the coordinated control of the hybrid powertrain during the EV/HEV mode transition. If the external disturbances are large, a high switching gain with a thicker boundary layer is required to reduce the resulting higher chattering effect. However, increasing the boundary layer thickness would reduce the feedback system to a system without the sliding mode [29,32]. Thus, in this study, a fuzzy adaptive inference system is developed to estimate the system disturbances. The overall coordinated control system scheme is shown in Fig. 4. In this figure, M_{en_tar}, M_{TM_tar}, M_{isg_tar}, and R_{cl_tar} are the target engine torque, the target TM torque, the target ISG torque, and the clutch command from the EMS, respectively; M_{en_cmd}, M_{TM_cmd}, M_{isg_cmd}, and R_{cl_cmd} are the engine torque command, the TM torque command, the ISG torque command, and the clutch command from the coordinated control strategy, respectively. The coordinated control strategy for the EV/HEV mode transition is developed according to the operating status of the clutch. Details of the coordinated control strategy will be presented in the following sections.

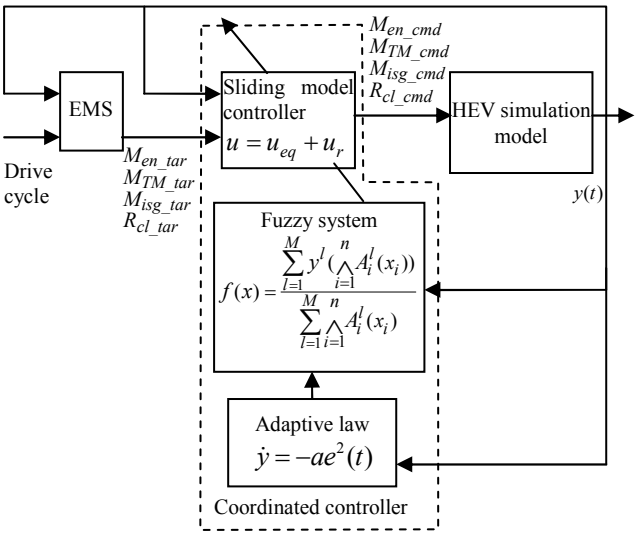

Fig. 4 Overall scheme of the coordinated control system

4.1 Control strategy when the clutch is unlocked

When the HEV is driven in the EV mode, the clutch is disengaged. During the transient process of the

EV/HEV mode transition, the clutch should initially be kept unlocked for engine cranking and speed synchronisation. In this phase, the engine is sped up to the ignition speed by the ISG with the maximum torque, and then, the coordinated control is utilised to regulate the ISG torque so that the engine speed is synchronised with the post-clutch speed.

During the synchronisation phase and because the clutch is unlocked, the TM torque command is directly given by the target torque from the EMS. To suppress the engine's transient operation and fuel enrichment, the engine throttle is restricted during the transition process, and the difference between the actual and target engine torques *d* is regarded as a disturbance to the drivetrain. The engine torque command during the coordinated control is given by Fig. 5. The ISG torque command is given by the overall control law of the fixed-boundary-layer sliding mode controller to ensure that the pre- and post-clutch speeds are synchronised. Therefore, the commands from the coordinated control strategy in this phase can be expressed as:

$$\begin{cases} M_{TM\_cmd} = M_{TM\_tar} \\ R_{cl\_cmd} = R_{cl\_tar} \\ M_{isg\_cmd} = u_1 \\ M_{en\_cmd} \ (see Fig.5) \end{cases} \tag{11}$$

where u_1 is the overall control law of the sliding mode controller. According to Eq. 7, the longitudinal dynamic equation for the input shaft of the clutch can be rewritten as:

$$\begin{aligned} &(J_{en\_isg} + J_{cl\_in})\ddot{\theta}_1 + b_{en\_isg}\dot{\theta}_1 = M_{en\_cmd} + d + u_1 \\ &where\ d_{\min} \le d \le d_{\max} \end{aligned} \tag{12}$$

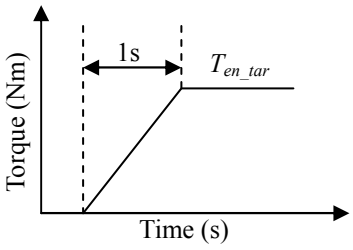

Fig. 5 Schematic of the engine torque command

To achieve the control objective, the overall control law of the SMC is determined by [28-32]:

$$u_1 = u_{eq1} + u_{r1} \tag{13}$$

where u_{eq1} is the equivalent control law, and u_{r1} is the reaching control law. To ensure that the pre- and post-clutch speeds are approaching synchronisation, let $\dot{\theta}_{1d} = \dot{\theta}_2$ be the desired trajectory. The synchronisation error e_1 can be defined as:

$$e_1 = \dot{\theta}_1 - \dot{\theta}_{1d} \tag{14}$$

Then, the sliding surface s_1 can be defined as:

$$s_1(t) = (\dot{\theta}_1 - \dot{\theta}_{1d}) + \lambda_1 \int_0^t (\dot{\theta}_1 - \dot{\theta}_{1d})dt \tag{15}$$

where λ_1 is a positive constant. When the closed-loop system is in the sliding mode, it satisfies $\dot{s}_1(t) = 0$, and the equivalent control law can be obtained using Eq. 16 according to Eq. 12:

$$u_{eq1} = b_{en\_isg}\dot{\theta}_1 - \hat{d} - M_{en\_cmd} + (J_{en\_isg} + J_{cl\_in})(\ddot{\theta}_{1d} - \lambda_1 e_1) \tag{16}$$

where $\hat{d}$ is the estimated value of *d*. In this study, a sat function is employed in the reaching control law to reduce the chattering. The sat function is defined as:

$$sat_1(s_1(t), \rho_1) = \begin{cases} \dfrac{s_1(t)}{\rho_1} & if\ |s_1(t)| < \rho_1 \\ \mathrm{sgn}(s_1(t)) & otherwise \end{cases} \tag{17}$$

where ρ_1 is the boundary layer thickness. Hence, the complete sliding mode control can be expressed as:

$$\begin{aligned} u_1 = {} & b_{en\_isg}\dot{\theta}_1 - \hat{d} - M_{en\_cmd} + (J_{en\_isg} + J_{cl\_in})(\ddot{\theta}_{1d} - \lambda_1 e) \\ & - \eta_1 sat_1(s_1) \end{aligned} \tag{18}$$

To approximate the disturbance *d*, a fuzzy adaptive inference system is utilised to estimate this parameter. For the fuzzy system, a TSK (Takagi-Sugeno-Kang) fuzzy inference engine is employed. The input linguistic variables of the fuzzy system are s_1 and $\dot{s}_1$, and a typical rule is as:

$R^m(t)$: IF $s_1(t)$ is A_1^m and $\dot{s}_1(t)$ is A_2^m, THEN $y^m(t)$ is $\hat{K}_m$.

where m=1,2,…,N is the index of the rule; A_i^m denotes the fuzzy sets assigned to the input variables; $\hat{K}_m$ denotes the fuzzy singletons assigned to the output $y^m(t)$ and is estimated by the adaptive law. Therefore, the disturbance *d* can be estimated by

$$\hat{d}(s(t), \dot{s}(t)) = (\hat{\mathrm{K}}(s_1(t), \dot{s}_1(t)))^T \cdot \Gamma(s_1(t), \dot{s}_1(t)) \tag{19}$$

where $\hat{K} = [\hat{K}_1, \hat{K}_2, ..., \hat{K}_N]^T$. $\Gamma = [\Gamma_1, \Gamma_2, ..., \Gamma_N]^T$, and Γ_i can be calculated by

$$\Gamma_i = \frac{A_1^i(s) \wedge A_2^i(\dot{s})}{\sum_{i=1}^{N} (A_1^i(s) \wedge A_2^i(\dot{s}))} \tag{20}$$

where $A_1^i(s)$ and $A_2^i(\dot{s})$ are the membership functions of *s* and $\dot{s}$, respectively.

The stability of the system (Eq. 12) with the control law (Eq. 18) is proved as follows. Define the following Lyapunov function:

$$V = \frac{1}{2}s_1^2 + \frac{1}{2}(\hat{K} - K^*)^T \cdot (\hat{K} - K^*) \quad (21)$$

where K^* is the optimal value of the adjustable parameter vector. The time-derivative of V is

$$\dot{V} = s_1 \cdot \dot{s}_1 + (\hat{K} - K^*)^T \cdot (\dot{\hat{K}} - \dot{K}^*) \quad (22)$$

By considering K^* to be a constant, we can obtain $\dot{K}^* = 0$. From Eq. 12 and Eq. 18, Eq. 22 can be rewritten as:

$$\begin{aligned}\dot{V} &= s_1\left(\frac{M_{en\_cmd} + u_1 + d - b_{en\_isg}\dot{\theta}_1}{J_{en\_isg} + J_{cl\_in}} - \ddot{\theta}_{1d} + \lambda_1 e\right) + (\hat{K} - K^*)^T \cdot \dot{\hat{K}} \\ &= \frac{s_1}{J_{en\_isg} + J_{cl\_in}}(d - \hat{d} - \eta_1 sat(s_1)) + (\hat{K} - K^*)^T \cdot \dot{\hat{K}}\end{aligned} \quad (23)$$

The minimum approximation error and the bound of the estimated parameter are defined as:

$$\begin{cases}\Delta_d = \hat{d}^* - d \\ \varepsilon_d = d_{\max} - d_{\min}\end{cases} \quad (24)$$

where Δ_d and ε_d are the minimum approximation error and the bound of the estimated parameter, respectively; $\hat{d}^*$ is the optimal estimate of d. Therefore, we can obtain:

$$\dot{V} = \frac{s_1}{J_{en\_isg} + J_{cl\_in}}(\eta_1 sat(s_1) + \Delta_d + (\hat{K} - K^*)^T \cdot \Gamma) + (\hat{K} - K^*)^T \cdot \dot{\hat{K}} \quad (25)$$

Let $(\hat{K} - K^*)^T \cdot \dot{\hat{K}} - \frac{s_1}{J_{en\_isg} + J_{cl\_in}}(\hat{K} - K^*)^T \cdot \Gamma = 0$ in Eq. 25.

Then, the adaptive law of the adjustable parameter vector is

$$\dot{\hat{K}} = \frac{s_1}{J_{en\_isg} + J_{cl\_in}}\Gamma \quad (26)$$

When $|s_1(t)| \geq \rho_1$, according to Eq. 17, Eq. 25, and Eq. 26, we can obtain:

$$\begin{aligned}\dot{V} &= -\frac{s_1}{J_{en\_isg} + J_{cl\_in}}(\eta_1 \operatorname{sgn}(s_1) + \Delta_d) \\ &\leq -\frac{|s_1|}{J_{en\_isg} + J_{cl\_in}}(\eta_1 - |\Delta_d|) \\ &\leq -\frac{|s_1|}{J_{en\_isg} + J_{cl\_in}}(\eta_1 - \varepsilon_d)\end{aligned} \quad (27)$$

Let $\eta_1 \geq \varepsilon_d$, then $\dot{V} \leq -k_1|s_1|$; $k_1 \geq 0$. Using the sliding mode theory [28,32], it can be concluded that the reaching condition $s(t) \cdot \dot{s}(t) < 0$ is satisfied and all the trajectories outside the boundary layer are attracted toward the boundary. It means that the system is stable and the error $|e_1| \leq 2\rho_1$ when $|s_1(t)| < \rho_1$.

4.2 Control strategy when the clutch is slipping

When the synchronisation error is less than 30 rpm, the clutch starts to be engaged and operates in the slipping status. The control objective in this phase is to ensure that the pre- and post-clutch speeds are fully synchronised. Therefore, the ISG torque command is also given by the overall control law of the sliding mode controller to ensure the pre- and post-clutch speeds synchronization. Because the clutch is slipping, the clutch friction torque is introduced to the drivetrain. The friction torque can be estimated by using the measured pressure. The difference between the actual and target engine torques is regarded as a disturbance to the drivetrain. Thus, the longitudinal dynamic equation for the input shaft of the clutch can be rewritten as:

$$(J_{en\_isg} + J_{cl\_in})\ddot{\theta}_1 + b_{en\_isg}\dot{\theta}_1 = M_{en\_cmd} + d + u_2 - M_{cl} \quad (28)$$

Meanwhile, the TM torque should be regulated to compensate for the clutch friction torque to avoid abrupt torque changes in the drivetrain. Thus, the commands from the coordinated control strategy in this phase can be expressed as:

$$\begin{cases}M_{TM\_cmd} = M_{TM\_tar} - \frac{1}{i_c}M_{cl} \\ R_{cl\_cmd} = R_{cl\_tar} \\ M_{isg\_cmd} = u_2 \\ M_{en\_cmd} \ (see\ Fig.5)\end{cases} \quad (29)$$

The tracking error e_2 and the sliding surface s_2 of the SMC in this phase are defined as:

$$\begin{cases}e_2 = \dot{\theta}_1 - \dot{\theta}_{1d};\ \dot{\theta}_{1d} = \dot{\theta}_2 \\ s_2(t) = (\dot{\theta}_1 - \dot{\theta}_{1d}) + \lambda_2\int_0^t(\dot{\theta}_1 - \dot{\theta}_{1d})dt\end{cases} \quad (30)$$

where λ_2 is a positive constant. According to Eq. 28 and Eq. 30, the complete sliding mode control can be expressed as:

$$\begin{aligned}u_2 = {} & M_{cl} + b_{en\_isg}\dot{\theta}_1 - \hat{d} - M_{en\_cmd} + (J_{en\_isg} + J_{cl\_in})(\ddot{\theta}_{1d} - \lambda_2 e_2) \\ & - \eta_2 sat_2(s_2)\end{aligned} \quad (31)$$

The derivation of the adaptive law and the proof of the stability of the system are similar to those in Section 4.1. Here, the adaptive law of the adjustable parameter vector is

$$\dot{\hat{K}} = \frac{s_2}{J_{en\_isg} + J_{cl\_in}}\Gamma \quad (32)$$

4.3 Control strategy when the clutch is locked

When the clutch is completely engaged, the

upstream and downstream parts of the clutch are locked together and spin at the same speed; meanwhile, the vehicle is driven by the three power sources simultaneously. In this phase, the control objective is to reduce vehicle jerk while satisfying the driver's torque request. Therefore, a reference model is utilised to provide the desired reference trajectory for the sliding mode controller. The dynamic equation of the reference model is

$$\begin{cases} (i_c^2 J_{TM} + J_c + J_{cl\_out} + \frac{1}{i_0^2} J_0 + J_{en\_isg} + J_{cl\_in})\ddot{\theta}_{2r} + (i_c^2 b_{TM} + \\ b_{en\_isg})\dot{\theta}_{2r} + \frac{1}{i_0} k_{da}(\frac{1}{i_0}\theta_{2r} - \theta_{3r}) + \frac{1}{i_0} b_{da}(\frac{1}{i_0}\dot{\theta}_{2r} - \dot{\theta}_{3r}) = M_D(\alpha) \\ J_{wh\_veh}\ddot{\theta}_{3r} = k_{da}(\frac{1}{i_0}\theta_{2r} - \theta_{3r}) + b_{da}(\frac{1}{i_0}\dot{\theta}_{2r} - \dot{\theta}_{3r}) - M_L \end{cases} \quad (33)$$

where α is the accelerator/brake pedal position; M_D is the driver's torque request; $\dot{\theta}_{2r}$ and $\dot{\theta}_{3r}$ are the engine and wheel speeds of the reference model. For the coordinated control in this phase, the ISG torque command is directly given by the target torque from the EMS, and the TM torque command is given by the overall control law of the SMC to achieve the control objective. Thus, the commands from the coordinated control strategy in this phase can be expressed as:

$$\begin{cases} M_{TM\_cmd} = u_3 \\ R_{cl\_cmd} = R_{cl\_tar} \\ M_{isg\_cmd} = M_{isg\_tar} \\ M_{en\_cmd} \ \ (see\, Fig.5) \end{cases} \quad (34)$$

The difference between the actual and target engine torques is regarded as a disturbance to the drivetrain. According to Eq. 9 and Eq. 34, we have

$$\begin{aligned} & J_{wh\_veh}\ddot{\theta}_3 + J_{eq}\ddot{\theta}_2 + (i_c^2 b_{TM} + b_{en\_isg})\dot{\theta}_2 + k_{da}(\frac{1}{i_0} - 1)(\frac{1}{i_0}\theta_2 - \theta_3) \\ & + b_{da}(\frac{1}{i_0} - 1)(\frac{1}{i_0}\dot{\theta}_2 - \dot{\theta}_3) + M_L = i_c u_3 + M_{en\_cmd} + M_{isg\_cmd} + d \end{aligned} \quad (35)$$

where $J_{eq} = i_c^2 J_{TM} + J_c + J_{cl\_out} + \frac{1}{i_0^2} J_0 + J_{en\_isg} + J_{cl\_in}$.

The tracking error e_3 and the sliding surface s_3 of the SMC in this phase are defined as:

$$\begin{cases} e_3 = \dot{\theta}_3 - \dot{\theta}_{3d};\ \dot{\theta}_{3d} = \dot{\theta}_{3r} \\ s_3(t) = (\dot{\theta}_3 - \dot{\theta}_{3d}) + \lambda_3 \int_0^t (\dot{\theta}_3 - \dot{\theta}_{3d})dt \end{cases} \quad (36)$$

where λ_3 is a positive constant. According to Eq. 35 and Eq. 36, the complete sliding mode control can be expressed as:

$$\begin{aligned} u_3 = & \frac{1}{i_c}(J_{eq}\ddot{\theta}_2 + (i_c^2 b_{TM} + b_{en\_isg})\dot{\theta}_2 + k_{da}(\frac{1}{i_0} - 1)(\frac{1}{i_0}\theta_2 - \theta_3) \\ & + b_{da}(\frac{1}{i_0} - 1)(\frac{1}{i_0}\dot{\theta}_2 - \dot{\theta}_3) + M_L + J_{wh\_veh}\ddot{\theta}_{3d} - J_{wh\_veh}\lambda_3 e_3 \\ & - M_{en\_cmd} - M_{isg\_cmd} - \hat{d}) - \eta_3 sat_3(s_3) \end{aligned} \quad (37)$$

The derivation of the adaptive law and the proof of the stability of the system are similar to those in Section 4.1. Here, the adaptive law of the adjustable parameter vector is

$$\dot{\hat{K}} = \frac{s_3}{J_{wh\_vel}}\Gamma \quad (38)$$

5 Simulation results and analysis

The proposed coordinated control strategy for the hybrid bus during the EV/HEV mode transition is tested by simulation over the CTBDC cycle to validate its effectiveness. In the simulation, a stretch of the CTBDC cycle is taken into account, and the EV/HEV mode transition occurs at 224.72 s, as shown in Fig. 6. The coordinated control is completed when $|M_{TM\_cmd} - M_{TM\_cmd}| \le 10$.

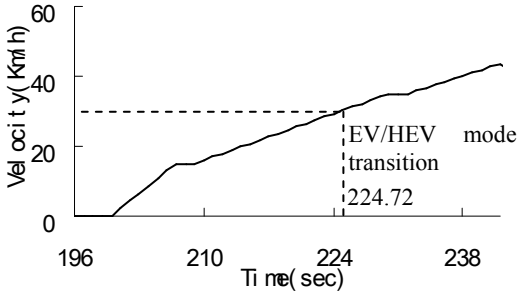

Fig. 6 A selected stretch of the CTBDC cycle

The simulation results without the coordinated control are shown in Fig. 7, and the simulation results with the proposed coordinated control strategy are shown in Fig. 8.

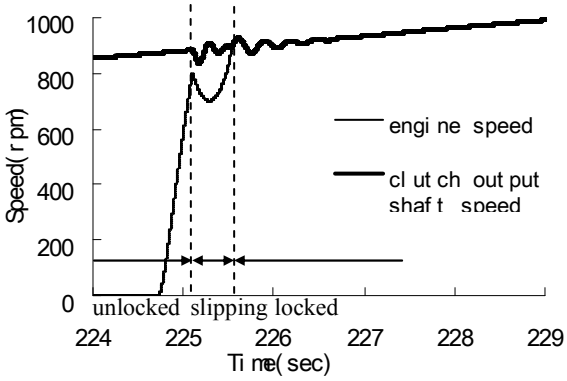

(a) Engine and clutch output shaft speeds

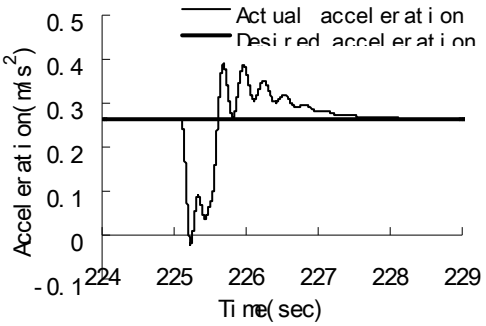

(b) Comparison of the actual acceleration with the desired acceleration

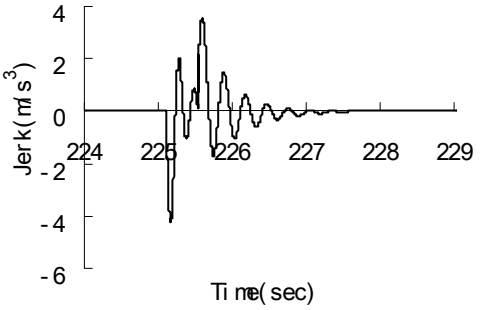

(c) Vehicle jerk

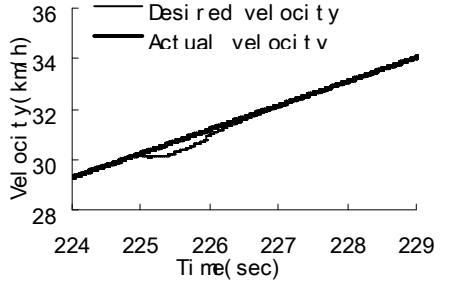

(d) Comparison of the actual velocity with the desired velocity

Fig. 7 Simulation results without the coordinated control

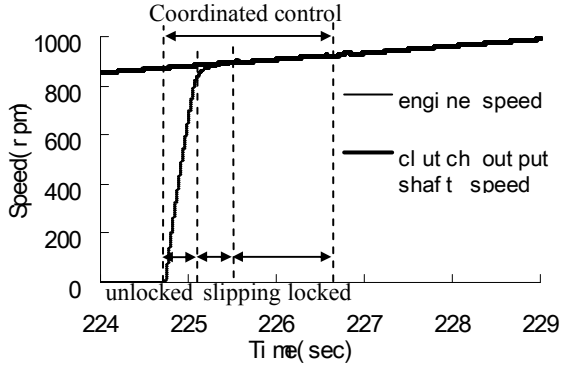

(a) Engine and clutch output shaft speeds

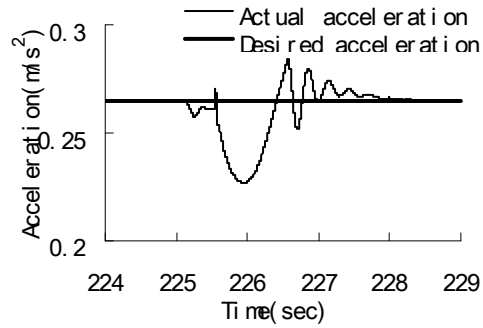

(b) Comparison of the actual acceleration with the desired acceleration

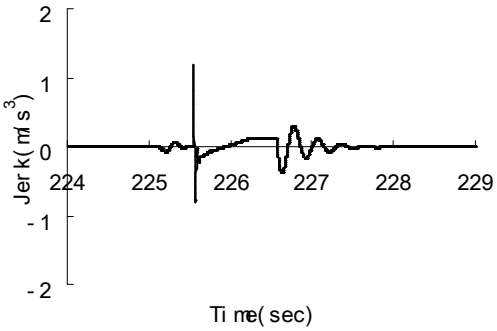

(c) Vehicle jerk

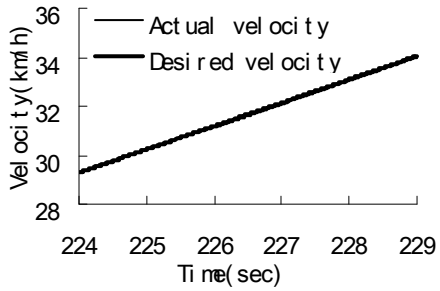

(d) Comparison of the actual velocity with the desired velocity

Fig. 8 Simulation results with the proposed coordinated control strategy

As is shown in Fig. 7, the control actions, which are directly given by the EMS, result in poor drivability during the transition from the EV mode to the HEV mode. The EMS is developed based on the static efficiency maps of the engine and the motors [33-35], and the transient characteristics of the power sources and the clutch are not considered. During the mode transition, the engine is sped up to 800 rpm by the ISG. Then, the engine is started and the clutch is engaged (at 225.08 s). Because of the torque response lag, the engine cannot output the target torque from the EMS, and the driver's torque request cannot be satisfied without coordinated control. Therefore, the engine speed and the vehicle acceleration drop sharply, and a significantly

negative jerk (-4.2 m/s^3) occurs, as shown in Fig. 7(a), Fig. 7(b), and Fig. 7(c). When the clutch is locked (at 225.53 s), the transmitted torque of the clutch changes from negative to positive; thus, the output shaft speed and the vehicle acceleration increase sharply, and a significantly positive jerk (3.8 m/s^3) occurs. Fig. 7(d) demonstrates that the velocity trajectory of the CTBDC cycle cannot be tracked during the transition without the coordinated control.

As is shown in Fig. 8, the simulation results demonstrate that the improvements in torque fluctuations and vehicle jerks during the EV/HEV mode transition can be achieved using the proposed coordinated control strategy. After the engine is started, the ISG is regulated by the coordinated control to synchronise the engine speed with the post-clutch speed. Meanwhile, the TM torque is regulated to compensate for the clutch friction torque to avoid abrupt torque changes in the drivetrain; thus, the driver's torque request can be satisfied. As is shown in Fig. 8(a), the engine speed increases while tracking the post-clutch speed. As is shown in Fig. 8(b), there is little error between the actual and desired accelerations, and the fluctuations in the vehicle acceleration are mostly suppressed. When the clutch is locked (at 225.55 s), the maximum vehicle jerk is reduced to 1.2 m/s^3 with the proposed coordinated control, as shown in Fig. 8(c). When $\left|M_{TM\_cmd}-M_{TM\_cmd}\right|\le 10$, the coordinated control is completed. The duration for the coordinated control is 1.88 s (224.72 s-226.6 s). After the coordinated control is completed, the control actions are given by the EMS, and the maximum vehicle jerk is less than 0.5 m/s^3. Fig. 8(d) demonstrates that the velocity trajectory of the CTBDC cycle can be tracked during the transition. It can be concluded that a smooth mode transition can be achieved using the proposed coordinated control strategy.

6 Conclusion

A coordinated control strategy based on the fuzzy adaptive sliding mode control was developed for a series-parallel hybrid electric bus to achieve a smooth transition from the EV mode to the HEV mode. The transient response characteristics of the engine and the motor as well as the friction-introduced discontinuity of the clutch torque were taken into account. A fuzzy adaptive inference system was developed to estimate the difference between the actual and desired engine torques. Then, the estimated torque difference was incorporated with a fixed-boundary-layer sliding mode controller to regulate the output torques of the ISG and the TM. The ISG torque was regulated for the pre- and post-clutch speeds synchronisation, and the TM torque was regulated to reduce the torque fluctuations of the powertrain. The proposed coordinated control strategy was developed according to the operating status of the clutch, and the engine throttle was restricted during the transition process to suppress engine's transient operation and fuel enrichment. When the difference between the target TM torque from the EMS and the TM torque command from the coordinated control strategy was less than 10 Nm, the coordinated control was completed. The proposed coordinated control strategy was implemented and tested in a forward-facing HEV model over the CTBDC cycle. The simulation results showed that the torque fluctuations and vehicle jerks during the EV/HEV mode transition can be reduced using the coordinated control strategy, and the CTBDC cycle can be tracked during the transition.

Acknowledgement

This research was supported by *The research and development of SWB6116 hybrid electric bus* (Grant No. 2006AA11A127, The National High Technology Research and Development Program of China).

References:

[1] Lino Guzzella, Antonio Sciarretta, *Vehicle Propulsion system*, Springer Berlin Heidelberg, 2007.

[2] C. M. Jefferson, R. H. Barnard, *Hybrid Vehicle Propulsion*, Computational Mechanics Inc., 2002.

[3] W. Scott Wayne, Nigel N. Clark, Ralph D. Nine, Dennis Elefante, A comparison of emissions and fuel economy from hybrid-electric and conventional-drive transit buses, *Energy & Fuels*, Vol. 18, pp. 257-270, 2004.

[4] Kazunari Moriya, Yoshiaki Ito, Yukio Inaguma, Design of the surge control method for the electric vehicle powertrain, *SAE International Congress & Exposition*, Detroit, USA, 2002, 2002-01-1935.

[5] Jeong Ho Hong, Seok Joon Kim, Byung Soon Min, Drivability development based on cosimulation of AMESim vehicle model and Simulink HCU models for parallel hybrid electric vehicle, *SAE International Congress & Exposition*, Detroit, USA, 2009, 2009-01-0725.

[6] I. D. Roy, D. L. Robert, Engine torque ripple cancellation with an integrated starter alternator

in a hybrid electric vehicle: implementation and control, *IEEE Transaction on Industry Application*, Vol. 6, pp. 2016-2018, 2003.

[7] Tong Yi, Li Jianqiu, Zhang Junzhi, Yang Fuyuan, Zhang Kexun, Yang Minggao, Coordinating control oriented research on algorithm of engine torque for parallel hybrid electric powertrain system, *SAE International Congress & Exposition*, Detroit, USA, 2004, 2004-01-0424.

[8] Feng Wang, Hu zhong, Zilin Ma, Power Distribution and coordinated control for a power split hybrid electric bus, *Journal of electric Engineering & Technology*, Vol. 3, pp. 593-598, 2008.

[9] K. Koprubasi, E. R. Westervelt, G. Rizzoni, Toward the Systematic Design of Controllers for Smooth Hybrid Electric Vehicle Mode Changes, *Proceedings of the 2007 American Control Conference*, New York, USA, 2007, pp. 2985-2990.

[10] Pierluigi Pisu, Kerem Koprubasi, Giorgio Rizzoni, Energy management and drivability control problems for hybrid electric vehicles, *2005 European control conference*, Seville, Spain, 2005, pp. 1824-1830.

[11] K. Koprubasi, M. Arnett, G. Rizzoni, Experimental Validation of a Model for Control of Drivability in a Hybrid-Electric Vehicle, *ASME 2007 International Mechanical Engineering Congress and Exposition,* Washington, USA, 2007, pp. 105-114.

[12] Zhao Zhiguo, He Ning, Zhu Yang, Yu Zhuoping, Mode Transition Control for Four Drive Hybrid electric Car, *Chinese Journal of Mechanical Engineering*, Vol. 4, pp. 100-109, 2011.

[13] H. D. Lee, S. K. Sul, Diesel engine ripple torque minimization for parallel type hybrid electric vehicle, *Thirty-Second IAS Annual Meeting*, New Orleans, LA, USA, 1997, pp. 942-946.

[14] Hyun Sup Kim, Ji Hun Him, Hyeong Cheol Lee, Mode transition control using disturbance compensation for a parallel hybrid electric vehicle, *Proceedings of the Institution of Mechanical Engineers Part D-Journal of Automotive engineering*, Vol. 2, pp. 150-166, 2009.

[15] J. P. Jensen, A. F. Kristensen, S. C. Sorenson, N. Houback, E. Hendricks. Mean value modelling of a small turbocharged diesel engine, *SAE International Congress & Exposition*, Detroit, USA, 1991, 910070.

[16] J. P. Jensen, A. F. Kristensen, S. C. Sorenson, N. Houback, E. Hendricks. Transient simulation of a small turbocharged diesel engine, *Proceedings of the Institution of Mechanical Engineers Seminar on Engine Transient Performances*, London, UK, 1990, pp. 31-43.

[17] Oscar Flardh, *Mean value modeling of a diesel engine with turbo compound*, Linkopings University, 2003.

[18] Argonne National Laboratory, *PSAT documentation*, Argonne National Laboratory, 2008.

[19] Chen Jiarui, *Automoblie Construction*, China Machine Press, 2007.

[20] V. V. Fernando, N. G. Rafael, B. M. Jose, Homemade RC ladder model of a thermopneumatic actuator, *WSEAS Transactions on Circuits and Systems*, Vol. 8, pp. 1220-1226, 2006.

[21] M. D. Oviatt, R. K. Miller, *Industrial Pneumatic Systems Control and Energy Conservation: Noise Control and Energy Conservation*, The Fairmont Press. Inc., 1981.

[22] Steffen Muller, Michael Uchanski, Karl Hedrick, Estimation of the maximum tire-road friction coefficient, *Journal of dynamic systems, measurement, and control*, Vol. 125, pp. 607-617, 2003.

[23] J. K. Hedrick, D. H. McMahon, D. Swaroop, Longitudinal vehicle control design for IVHS systems, *Proceedings of the 1991 American Control Conference*, Boston, USA, 1991, pp. 3107-3112.

[24] D. H. McMahon, J. K. Hedrick, S. E. Shladover, Vehicle Modelling and Control for Automated Highway Systems, *Proceedings of the 1990 American Control Conference*, San Diego, USA, 1990, pp. 297-303.

[25] V. H. Johnson, Battery performance models in ADVISOR, *Journal of Power Source*, Vol. 8, pp.321-329, 2002.

[26] Ryan A. McGee, Model based control system design and verification for a hybrid electric vehicle, *SAE International Congress & Exposition*, Detroit, USA, 2003, 2003-01-2308.

[27] Lei Wang, Yong Zhang, Chengliang Yin, Hardware-in-the-loop simulation for the design and verification of the control system of a series-parallel hybrid electric city-bus, *Simulation Modelling Practice and Theory*, Submitted, 2011.

[28] P. Kachroo, M. Tomizuka, Chattering reduction and error convergence in the sliding-mode control of a class of nonlinear system, *IEEE Transactions on Automatic Control*, Vol. 7, pp. 1063-1068, 1996.

[29] M. Roopaei, M. Zolghadri, S. Meshksar,

Enhanced adaptive fuzzy sliding mode control for uncertain nonlinear systems, *Commun Nonlinear Sci Numer simulate*, Vol. 14, pp. 3670-3681, 2009.

[30] Jie Shu, Yong Zhang, Chengliang Yin, Longitudinal control of hybrid electric buses using traction motor and pneumatic braking system, *WSEAS Transactions on Circuits and Systems*, Vol. 8, pp. 873-882, 2009.

[31] S. Wirote, S. Sarawut, Adaptive sliding-mode speed-torque observer, *WSEAS Transactions on Systems*, Vol. 5, pp. 458-466, 2006.

[32] J. J. Slotine, W. P. Li, *Applied nonlinear control*, Prentice-Hall Englewood Cliffs, 1991.

[33] Farzad Rajaei Salmasi, Control Strategies for Hybrid Electric Vehicles: Evolution, Classification, Comparison, and Future Trends, *IEEE Transactions on Vehicular Technology*, Vol. 5, pp. 2393-2404, 2007.

[34] Chan Chiao Lin, Huei Peng, Jessy W. Grizzle, Power Management Strategy for a Parallel Hybrid Electric Truck, *IEEE Transactions on Control Systems Technology*, Vol.11, pp. 839-849, 2003.

[35] Wang Lei, Zhang Jianlong, Yin Chengliang, Zhang Yong, Realization and Analysis of Good Fuel Economy and Kinetic Performance of a Low-cost Hybrid Electric Vehicle, *Chinese Journal of Mechanical Engineering*, Vol. 5, pp. 774-789, 2011.